ACSNANO

www.acsnano.org

ARTICLE

Temperature-Regulated Bidirectional Capillary Force Self-Assembly of Femtosecond Laser Printed Micropillars for Switchable Chiral Microstructures

Dong Wu, Caiding Ni, Zhaoxin Lao,* Yang Cao, Jincheng Ni, Zhongguo Ren, Shunli Liu, Yuan Tao, Chen Xin, Deng Pan, Yanlei Hu,* and Jiaru Chu

Cite This: https://doi.org/10.1021/acsnano.3c04181

Read Online

ACCESS | Metrics & More | Article Recommendations | Supporting Information

ABSTRACT: **Bottom-up self-assembly is regarded as an alternative way to manufacture series of microstructures in many fields, especially chiral microstructures, which attract tremendous attention because of their optical micromanipulations and chiroptical spectroscopies. However, most of the self-assembled microstructures cannot be tuned after processing, which largely hinders their broad applications. Here, we demonstrate a promising manufacturing strategy for switchable microstructures by combining the flexibility of femtosecond laser printing induced capillary force self-assembly and the temperature-responsive characteristics of smart hydrogels. Through designing asymmetric cross-link density, the printed microarchitectures can be deformed in the opposite direction and assembled into switchable ordered microstructures driven by capillary forces under different temperatures. Finally, the assembled chiral microstructures with switchable opposite handedness are realized, which shows tunable vortical dichroism. The proposed strategy holds potential applications in the fields of chiral photonics, chiral sensing, and so on.**

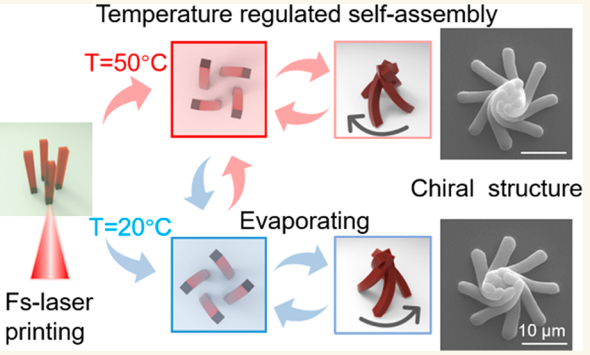

KEYWORDS: *self-assembly, capillary forces, chiral microstructures, femtosecond laser, two photon polymerization*

In recent years, bottom-up self-assembly driven by some weak forces (e.g., van der Waals force,[1] electrostatic force,[2] capillary force, surface tension[3]) has attracted extensive attention in order to fabricate microstructures with outstanding optical and mechanical properties. Among manifold weak forces, capillary force is widely used for self-assembly due to its distinctive advantages including simplicity, scalability, and low cost.[4,5] Through the capillary force generated by a meniscus during liquid evaporation, two-dimensional or three-dimensional complex structures can be self-assembled from microparticles,[6−8] micropillars,[9,10] microwalls/microchannels,[11,12] or films.[13−17] Direct laser writing (DLW) has a high degree of freedom and flexibility and has a high spatial resolution in the preparation of 2D−3D micro−nanostructures,[18,19] which can be further transformed into hierarchical functional structures by capillary force assembly. So, femtosecond laser printing induced capillary force self-assembly (LPCS) combines the advantages of the two above, making it a promising tool in the fabrication of complex 3D microassemblies.[20,21] LPCS can produce ordered hierarchical microstructures efficiently and stably for the selective capture and release of objects. LPCS is also used to prepare nanogap plasmonic microstructures, which could be used for SERS detection. In addition, microassemblies with adjustable spacing are fabricated on a flexible substrate to realize multifunctional object capture and intelligent display. Although LPCS has been applied in fabricating various microstructures for particle trapping[10] and SERS sensing,[22] there are few reports on the facile preparation of flexible and tunable chiral microstructures.

As we all know, chirality is a delicate and ubiquitous phenomenon in nature, including thread,[23] DNA double

Received: May 10, 2023
Accepted: June 20, 2023

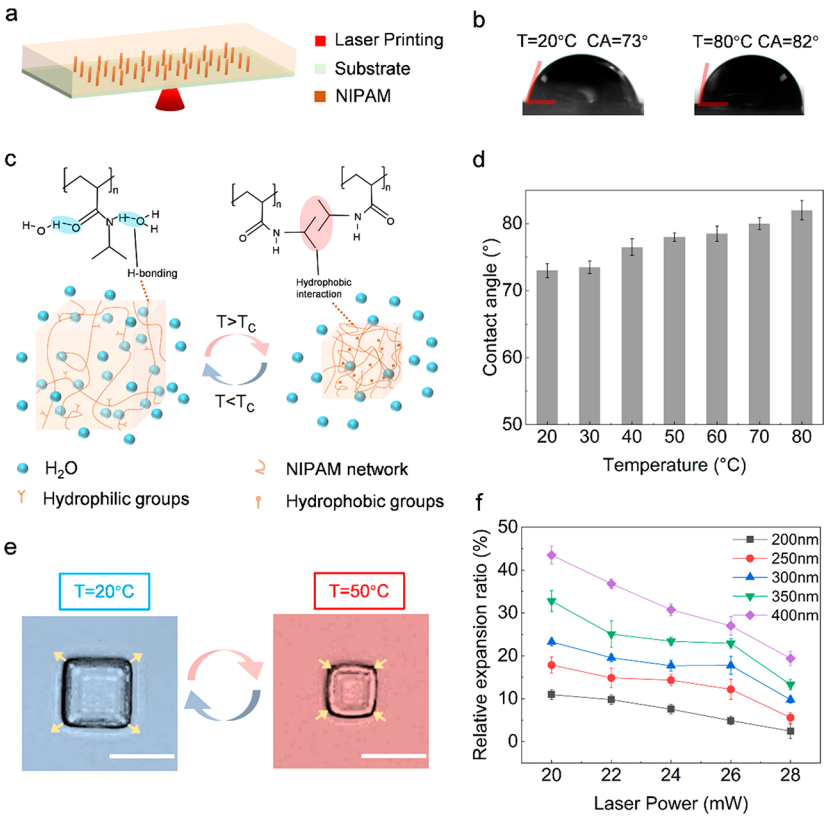

Figure 1. Properties of temperature-responsive hydrogels. (a) Schematic diagram of hydrogel micropillar arrays fabricated by femtosecond laser processing. (b) The contact angle (CA) of NIPAM at different temperatures. (c) The hydrogel polymer chain has hydrophobic and hydrophilic domains. (d) The average CA increases when the temperature increases. (e) The hydrogel blocks expand and contract in volume at 20 and 50 °C, respectively. (f) Quantitative relationship between laser power and relative expansion of the hydrogel blocks at different laser-scanning steps. Scale bars: 10 μm.

molecular chain,[24] tendons,[25] ligaments,[26] and tendrils of clinging plants.[27] The chiral microstructure itself has a hand-light effect, which endows it great application prospects in the detection of biomolecules and thus attracts tremendous attention in biomedicine.[28] It has been possible to assemble mesoscale bristles to form ordered helical clusters under the action of capillary forces by photolithography,[29] but the chirality of the formed microstructures is random. The previous works mostly focused on designing the geometry and spatial arrangement of micropillars to generate asymmetric capillary forces, which can cause them to assemble into a chiral structure in a controlled manner,[20] but the chirality of the processed microstructure is definite and unchangeable after processing. Therefore, it is still a great challenge to form reversible, controllable, and transparent chiral microstructures in an efficient fashion.

In order to achieve chiral switching, the stimuli-response properties of smart materials can be utilized. Smart hydrogels that can rapidly change their properties when the external environment (such as temperature, humidity, pH value, ionic strength, light conditions) varies[30] have captured a sea of interest in many fields, such as microactuators,[31] microvalves,[32] cell tissue engineering,[33] drug delivery mediators, artificial muscles, and soft biomimetic robots.[34,35] Femtosecond DLW can achieve complex three-dimensional morphologies with smart hydrogel materials. Smart hydrogels deform by shrinking or expanding, and the degree of deformation of the hydrogel can be regulated by changing laser processing parameters such as the scanning distance, energy, and exposure time.[18] In particular, temperature as a stimulus is of great interest, because it is easily changeable. By using two-photon polymerization for processing stimuli-responsive hydrogels, the active structures that show a large-amplitude response to temperature changes have been achieved.[36] Based on temperature-responsive hydrogels, Qian et al. reported a phototropic system that can aim and align to the three-dimensional direction of incident light over a wide range of temperatures.[37] Although the preparation and actuation of temperature-responsive hydrogels have been extensively studied, the hydrogel microstructures capable of rapid chiral switching still remain to be explored.

Herein, we introduce a responsive hydrogel-based LPCS strategy to fabricate the reversible regulated hierarchical functional structure that cannot be achieved by traditional LPCS. By using the deformation difference of the hydrogel with different cross-linking densities, a switchable chiral self-assembly is prepared, in which the chirality can reversibly switch between opposite directions by temperature. The assembly process of chiral structures at different temperatures is studied, and high repeatability is demonstrated. By studying the difference in the reflection intensity of light with opposite orbital angular momentums on the chiral structures, the potential applications in the field of chiral photonics are showcased.

RESULTS AND DISCUSSION

As shown in Figure 1a, a femtosecond laser beam is focused into a hydrogel material for fabricating micropillars. The

https://doi.org/10.1021/acsnano.3c04181
ACS Nano XXXX, XXX, XXX−XXX

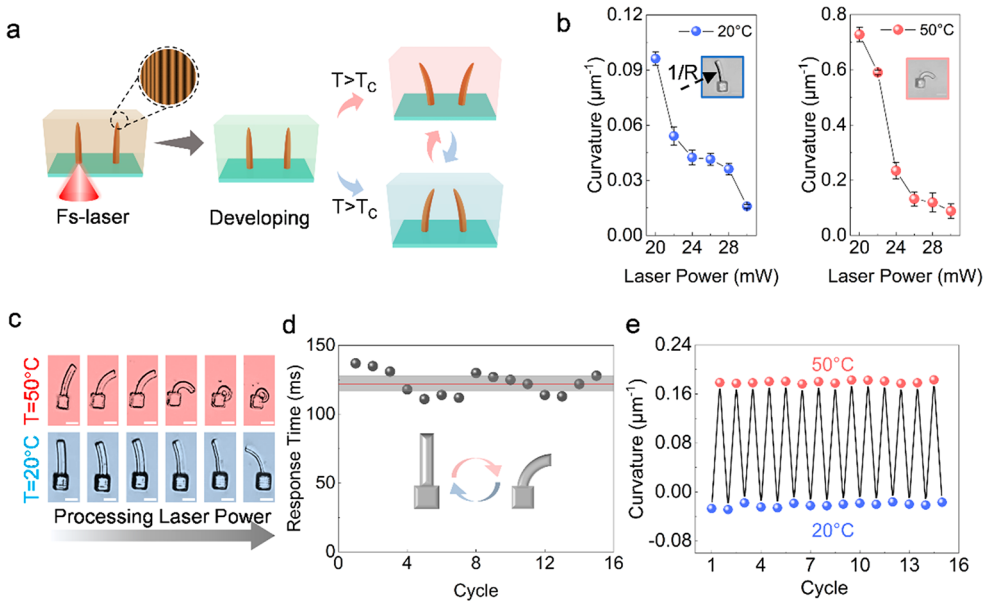

Figure 2. The concept of dynamically controllable bidirectional bending of hydrogel micropillars at different temperatures. (a) Schematic diagram of bidirectional bending of laser-processed hydrogel micropillars. The enlarged image shows different scanning steps on the cross section of hydrogel micropillars. (b) Bending curvature of hydrogel cantilevers with different laser powers at 20 and 50 °C, respectively. (c) The corresponding optical images of hydrogel cantilevers with different laser powers. (d) The characterization of dynamical response time of the cantilever by changing the temperature. (e) Repeatability verification of cantilever curvature at 20 and 50 °C. Scale bars: 10 μm.

material is a kind of temperature-sensitive hydrogel, NIPAM (N-isopropyl acrylamide), which is mainly composed of *N*-isopropylacrylamide, *N*,*N*′-methylenebis(acrylamide), and diphenyl(2,4,6-trimethylbenzoyl) phosphine oxide. The polymer network inside the hydrogel contains hydrophilic and hydrophobic groups, which means the contact angle (CA) of the hydrogel changes at different temperatures (Figure 1b,d). Figure 1d expresses that the CA increases as the temperature increases from 20 °C to 80 °C. The change of temperature affects the interaction between these groups and water molecules, so that the pores of the hydrogel change, which leads to volume contraction/expansion. When the ambient temperature is below the critical temperature (T_C), strong hydrogen bonding between hydrophilic groups and water molecules makes the thermosensitive hydrogel expand (Figure 1c). On the contrary, hydrogen bonding weakens, while the hydrophobic groups' interaction is strengthened, which leads to the volume contraction of hydrogels.[38]

For subsequent assembly structure design, the expansion and contraction characteristics of this thermally responsive hydrogel are studied, and a cube block (side length L = 10 μm) is designed to observe the deformation under different conditions (Figure 1e). When the developed block is put into deionized water at 20 °C, the side length of the square will be slightly larger than 10 μm due to expansion. After that, when put into deionized water at 50 °C, the structure shrinks rapidly (the details of the solution temperature change are provided in Supporting Information Figure S1). In short, once the solution temperature changes beyond T_C, the response time of the hydrogel structure is at the subsecond level. To characterize the deformation range of the thermally responsive hydrogels during the swelling−deswelling process, the relative expansion ratio (RER) defines the ratio of the length difference between the expanded and contracted states to the length in the contracted state:

$$\mathrm{RER} = \frac{L_{\mathrm{expansion}} - L_{\mathrm{contract}}}{L_{\mathrm{contract}}}$$

Therefore, the RER reflects the relative deformability of the structure. As shown in Figure 1f, by changing the parameters of laser processing, the range of the RER can be adjusted. It can be seen that when the hatching distance is fixed, the RER decreases as the laser power increases. When the power is 20 mW, with the increase of the hatching distance (*hd*) (from 200 to 400 nm), the RER always increases. The RER reaches the maximum value of 0.43 when *hd* reaches 400 nm. The reason is that the degree of cross-linking of the hydrogel affects its swelling properties. While the *hd* is >400 nm, the power density may be too small to fabricate microstructures.

The hydrogel building block was processed into two asymmetric parts with a width ratio of 3:7, and different cross-linking densities were achieved by imparting different hatching distances (150 nm for the areas with higher cross-linking density and 350 nm for the areas with lower cross-linking density) (Figure 2a). After photopolymerization, the sample was developed in ethanol for about 5 min to remove unpolymerized monomers or oligomers so that the microstructures fabricated by laser scanning are left on the slide substrate. When the development completed, as shown next in Figure 2a, the structure is immersed in solution with different temperatures (below and above T_C, respectively). Due to the responsive properties of NIPAM with asymmetric cross-linking densities, the micropillars have different bending directions at different temperatures.

In order to further understand the deformation of large aspect ratio structures, we designed an asymmetric cantilever beam structure, where the length of the beam part is 30 μm and the diameter of the cross section is 6 μm (Figure 2c). The curvatures of the cantilever beam at different temperatures are measured (Figure S2). When the temperature is lower than 40 °C, the curve is always in an upward trend. Then the curve

https://doi.org/10.1021/acsnano.3c04181
ACS Nano XXXX, XXX, XXX−XXX

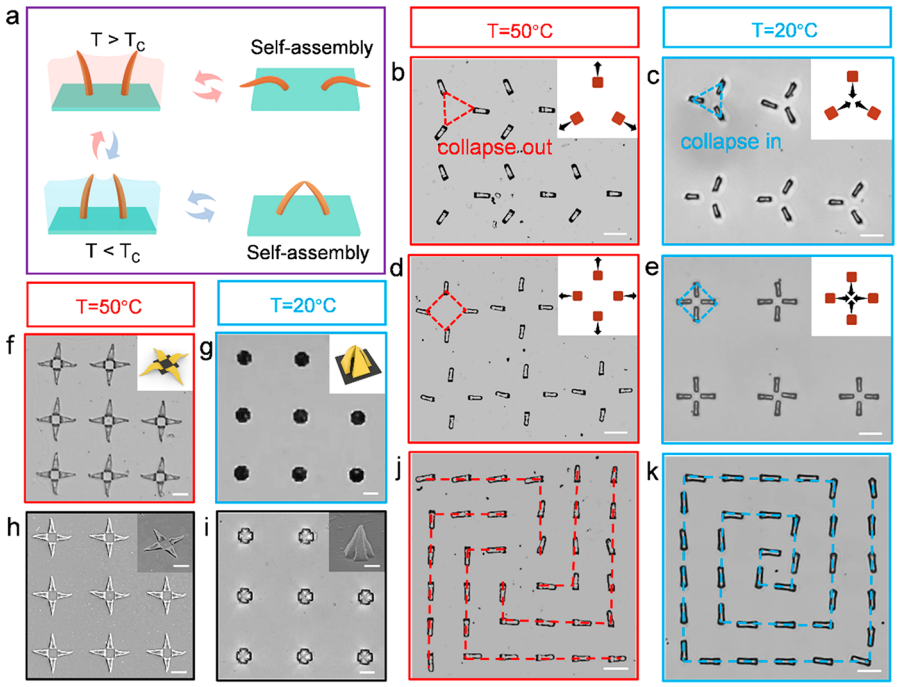

Figure 3. Controllable patterns of temperature-regulated bidirectional assembly. (a) Bidirectional bending volatilization process diagram. (b, c) Optical images of 3-fold symmetric micropillars collapsing out at 50 °C (b) and collapsing in at 20 °C (c). (d, e) Optical images of 4-fold symmetric micropillars collapsing out at 50 °C (d) and collapsing in at 20 °C (e). (f, g) Optical images of microgripper opening and closing in the air. (h) Scanning electron microscopic image of microgripper opening. (i) Optical images of microgripper closing in the liquid. (j, k) Bidirectional bending assembly of ring arrays. Scale bars: 20 μm.

becomes stable when it reaches 40 °C. This can prove that the critical deformation temperature of the temperature-responsive hydrogel used is in the range 30−40 °C. In our study, 50 °C is adopted as the experimental temperature above T_C. Due to the existence of anisotropy, the newly developed structure absorbs water and expands at room temperature, which bends in one direction. When placed in an aqueous solution of 50 °C, the cantilever instantly bends in the opposite direction. We use a high-speed camera to photograph the bending process of the cantilever beams and record the response time. After multiple measurements, the average response time is 127 ms (<200 ms) (Figure 2d, Supporting Information Figure S3 and Video V1). Figure 2d shows the bending of cantilever beams processed by different laser powers, above and below T_C. Moreover, the dehydrated hydrogels also have a certain anisotropy, and the cantilever beams fabricated with different laser powers have different bending curvatures after dehydration (Supporting Information Figure S9). Figure 2b records the curvature of the cantilever beams at different temperatures (20 and 50 °C), which are fabricated with different energies in the range of 20−30 mW, respectively. The curvature of the shrinkage bending of the hydrogel is 1 order of magnitude larger than the swelling bending. To evaluate the fatigue resistance of the hydrogel, the curvature of the cantilever is measured during multiple contraction and expansion bending, validating the repeatability of the thermally responsive hydrogel (Figure 2e).

Due to the characteristic of bidirectional bending under different conditions, the design of various 2D and 3D structures is inspired based on this reversible bidirectional bending property. The evaporation of the solution induces a net capillary force to bend the anisotropic micropillar structure toward the curving direction[39−41] (the mechanical analysis is shown in Supporting Information Figure S4). Therefore, for the same structure, by using solution environments of different temperatures, the structure realizes reversible bidirectional changes, which enrich the traditional unidirectional assembly (Supporting Information Figure S5). In the final stages of assembly, as the solution evaporates and reaches the top of the structural unit, a meniscus forms inside the unit cells as well as between the unit and the base surface, respectively. Capillary forces directed by the meniscus pull the building blocks into two morphologies: (i) assembly; (ii) attached to the base. Using this bidirectional bending property, we can construct a variety of patterns (Figure 3a). As shown in Figure 3b−3e and Supporting Information Figure S12, three micropillar units and four micropillar units were designed with the same height (20 μm). Each structure is placed in an aqueous solution environment at different temperatures, so that there will be two forms, “Ccollapse in” and “collapse out”. Besides, the co-directional array proves that orderly patterns can be fabricated in large quantities (Supporting Information Figure S12). However, due to the high degree of cross-linking, the micropillars are unable to collapse (Supporting Information Figure S13). Then, the ring structure is also designed (Figure 3k). Figure 3j is the reverse of the ring structure; although the ring is destroyed, it conforms to the bending direction of the ideal structure. Similarly, tunable microplates or microwalls can also be prepared for the bidirectional assembly in this way (Supporting Information Figure S10). In addition to this, we also prepared a microgripper, which is equipped with capture, encapsulation, and sensing capabilities, to cope with the complex environments (inset in Figure 3g). The height of the microgripper is 30 μm, and the distance between the opposite fingers is 20 μm. Here, by simulating the change of ambient temperature, we realize the closing and opening of the microgripper (Figure 3f−3i and Supporting Information Figure

https://doi.org/10.1021/acsnano.3c04181
ACS Nano XXXX, XXX, XXX−XXX

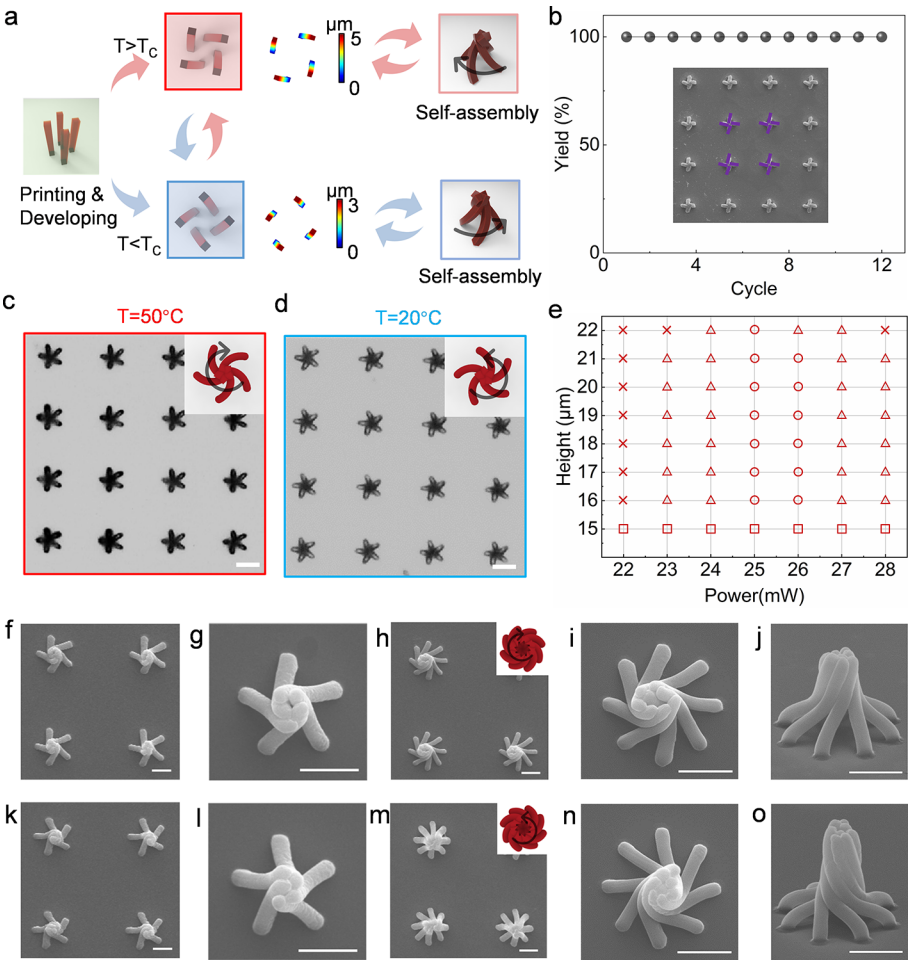

Figure 4. Demonstration of temperature-regulated chiral assemblies. (a) Assembly process diagram and simulation diagram of different chiral structures. In addition, the four-pillar unit is simulated under different temperatures, and the degree of deformation increased gradually from blue to red. Blue means small deformation; red means large deformation. (b) The production yield of the assembly in an array. (c, d) Optical images of a bidirectionally assembled 5-p assembly. (e) Phase diagram of component modes with different column heights and laser powers. The circular area represents the appropriate set of parameters for the formation of the four-column chiral combination. □: standing, ×: collapsed and cannot be self-assembled, ○: successfully self-assembled, △: only part can be self-assembled. (f, g, k, l) Top view of electron microscopic images of 5-p structures with different handedness. (h–j, m–o) Top (h, i, m, n) and side (j, o) views of electron microscopic images of 8-p structures with different handedness. Scale bars: 10 μm.

S11). The switching of the two morphologies increases the flexibility of the microgripper, which can be used for object capture and controlled release.

Through the design concept of anisotropic micropillar elements and spatial topology, we try to construct some chiral structures with a certain complexity. Using the different bending directions of micropillars under different temperature environments, we constructed a structure to reversibly switch chirality. Compared with the limitation of the traditional self-assembly of one structure, which can only have one chirality, this work has breakthroughs and innovations. As shown in Figure 4a and Supporting Information Figure S6, the printed micropillars are placed in an aqueous solution with a temperature lower than T_C, and the micropillar unit is left-handed. After the solution evaporates, the micropillars collapse around the center of rotation, and a structure with left-handedness is generated. Then, by placing the structure in solution with a temperature higher than T_C, the micropillars can stand again and bend in the other direction. After being evaporated on a heating plate, the micropillars assemble into a right-handed chiral structure (Video V2), which realizes the chiral switch. The switching time of a chiral microstructure is about 0.8 s (Figure S7). In order to understand the deformation process of the structure more intuitively, we simulate the bending directions of the micropillars in water at different temperatures. It can be seen that under the stimulation of different temperatures the units have different chirality prototypes. Repeated assemblies are performed to demonstrate the reversibility and repeatability of temperature-regulated capillary assembly (Figure 4b). The success rates are all 100% in the experiment, indicating that the reliability of the microstructures is excellent. In addition, we also have assembled, disassembled, and reassembled the five-pillar units in 15 cycles, and the microstructures still show good assembly morphology (Figure S8). Therefore, the chiral microstructures prepared by our strategy have good fatigue resistance and can be reused.

In order to precisely control the morphology of self-assembly, the influence of relevant important parameters in the printing process and mutual constraints between them are explored. Among many parameters, the height of the micropillars and the power of the laser processing play crucial

https://doi.org/10.1021/acsnano.3c04181
ACS Nano XXXX, XXX, XXX–XXX

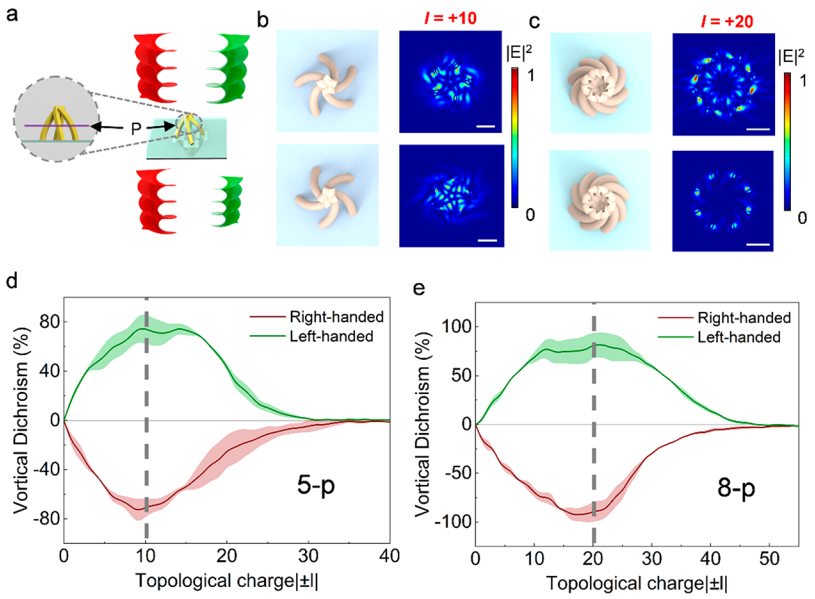

Figure 5. Vortical dichroism measurements of the reversible chiral assemblies. (a) Schematic diagram of an OAM beam vertically illuminated on a chiral structure (plane P is the cross-section selected by simulation). (b, c) Electromagnetic simulations of the chiral microstructures assembled by five and eight micropillars. Distinguished cross-sectional electric field distributions are generated for chiral microstructures with opposite handedness. (d, e) The optical vortical dichroism spectra for chiral microstructures consisted of different micropillars: (d) 5-p chiral assemblies, (e) 8-p chiral assemblies. Scale bars: 10 μm.

roles in the assembly. It can be seen that when the energy is lower than 24 mW or higher than 27 mW, the success rate of assembly is relatively lower, and the success rate between 25 and 26 mW is higher (Figure 4e). This is because when the energy is too high (>28 mW), the rigidity of the structure is large, and its own elastic force is greater than the capillary force, resulting in the micropillars in the standing state. On the contrary, when the energy is too low (<23 mW), the micropillars eventually collapse due to their low stiffness. The successful assemblies of five-pillars whose height is 20 μm and fabrication energy is 26 mW are shown in Figure 4c,d. The distance from each pillar to the center of rotation of the unit is 4 μm. The chirality of the five-pillar units (Figure 4f,g,k,l) is greater than the four-pillar units (Supporting Information Figure S14). When the pillar number of assemblies increases to 8, the distance from each pillar to the center of rotation of the unit and height of the pillars are designated as 6 and 22 μm, respectively, to make the spacing suitable for self-assembly (Figure 4h,i,j and Figure 4m,n,o). Further, eight-pillar units are twisted more than five-pillar units. From five-pillar units to eight-pillar units, they all exhibit varying degrees of different handed chiral structures due to bidirectional assembly. From the top view of the assembly, all the assembled units are highly ordered and rotationally symmetric, and each micropillar is continuously superimposed around the center of rotation to form an interlocking structure. It is worth noting that after optimizing the parameters including the processing power, exposure time, and hatching distance, smaller chiral assemblies can be achieved. As proof, three-pillar assemblies with a size of 3−4 μm were realized, in which the stacked area at the top part of the assembly is about 1 μm. Compared with rigid materials such as photoresist, the chiral assembly in our work prepared by a temperature-sensitive hydrogel has significant distortion (Figure S15).

Artificial chiral micro/nanostructures fabricated by many top-down or bottom-up methods have been widely used in chiroptical responses and enhancing chiral molecules sensing. The vortical dichroism (VD)[20,42] is typically considered an intrinsic property of chiral micro/nanostructures. The chiroptical signals are invariable for the engineered chiral micro/nanostructures. Here, we investigate the switchable chiroptical responses of the hydrogel micropillars. To characterize the chiroptical signals, the VD can be defined as

$$\mathrm{VD} = 2 \times \frac{I_R - I_L}{I_R + I_L}$$

where I_R and I_L are the reflection intensities of helical microstructures under right-handed wavefront (RHW) and left-handed wavefront (LHW) illumination, respectively. As shown in Figure 5a, the corresponding VD spectra of left- and right- handed chiral microstructures were measured by vertical illumination of vortex beams with different topological charges. We simulate the electromagnetic fields of the chiral microstructures illuminated by vortex beams with topological charge l = +10 (Figure 5b). It is obvious that the electric field distribution is dependent on the chirality of the micropillars, implying a chiroptical response. Similar characterization can also be found in 8-fold symmetric micropillars, where a strong interaction is generated by vortex beams with a large topological charge l = +20 (Figure 5c). To confirm our prediction, we measured the VD spectra of 5- and 8-fold symmetric micropillar units with opposite handedness, as shown in Figure 5d,e. Obviously, all the VD spectra are basically mirror-symmetrical along the VD = 0 lines, which indicates that they have opposite chirality by changing temperature. The peak value of five-pillar units reaches around 60% when the topological charge is 10, while the peak value of eight-pillar units reaches around 80% when the topological charge is 20. Since the overall size of the eight-pillar unit is larger than that of the five-pillar unit, the peak of VD spectra can move toward larger topological charges and possess a strong VD response accordingly. When the diameter of the

https://doi.org/10.1021/acsnano.3c04181
ACS Nano XXXX, XXX, XXX−XXX

vortex light is larger than the diameter of the structure, the annular vortex beam is separated from the surface of the chiral structure, resulting in zero VD value. The VD peaks of opposite-handed microstructures have slight asymmetry, which can be ascribed to the inconsistencies of the height of the chiral structures after self-assembly. In short, distinct from the fixed chirality of artificial structures, we demonstrate the controlling chiroptical responses of the switchable chiral structures fabricated by our method.

CONCLUSIONS

In summary, a switchable capillary-force self-assembly strategy based on a temperature-responsive hydrogel is proposed to construct 2D and 3D microstructures. Using the deformation differences of different cross-linking densities in the smart hydrogel, the reversible switching self-assembly of chiral microstructures between the opposite directions is prepared. The complexity and regularity of the assembly demonstrate great prospects for the preparation of chiral microstructures over a large range. Furthermore, the fast response (200 ms) of temperature-responsive hydrogels also promotes the rapid switching of self-assemblies. The temperature-regulated chiral self-assembly exhibits a good chiral tunable property through the analysis of the results of VD spectra, which are basically mirror-symmetrical along the VD = 0 lines. In addition, the differences in vortical dichroism of different patterned self-assemblies are revealed. In the future, spatial light modulation, which greatly improves the efficiency of laser direct writing,[43,44] can also be employed in the fabrication of switchable chiral microstructures. This stimuli-regulated LPCS technique based on smart materials to prepare tunable chiral microstructures will show broad potential applications in optical sensing, particle manipulation, and microfluidic trapping.

EXPERIMENTAL SECTION

Material. The main materials used in the experiment are *N*-ropylacrylamide, *N*,*N*′-methylenebis(acrylamide), diphenyl(2,4,6-trimethylbenzoyl) phosphine oxide, which are used to prepare hydrogels. Other material is deionized water to provide a solution environment. The resist is prepared by dissolving 400 mg of *N*-isopropylacrylamide, 30 mg of *N*,*N*′-methylenebis(acrylamide), 30 mg of diphenyl(2,4,6-trimethylbenzoyl) phosphine oxide, and 50 mg of polyvinylpyrrolidone K30 into 450 μL of ethylene glycol. In addition, a small amount of Rhodamine 6G is needed for the dyeing treatment.

Experimental Setup. Before processing the hydrogel, it needs to be dropped onto the treatment slide; then we need to bake it on a hot plate for 5−10 min. Next, we fix the sample on the piezoelectric table and control the mirror to perform point-by-point processing through the program. The maximum area of the processed arrays is 200 μm × 200 μm. The laser source used in this experiment is a sapphire ultrafine oscillator (80 MHz), whose central wavelength is 800 nm and pulse duration is 75 fs. In addition, an oil-immersed objective lens (60×, NA = 1.35, Olympus) is used to focus the laser beam to change the degree of polymerization of the hydrogel. By importing the three-dimensional coordinates generated by MATLAB into the control software system, the corresponding path of mirror processing is controlled. The sample is immobilized on a 3D nanotranslation platform with nanoresolution and a mobility range of 200 μm × 200 μm × 200 μm.

Capillary Force Induced Self-Assembly. After the structure is printed, it is developed in ethanol solution for 10 min to remove unpolymerized material. Then it is removed from ethanol and placed in deionized water at 20 and 50 °C, respectively. After the deionized water evaporates, the printed anisotropic micropillar array forms three-dimensional chiral microstructures with different rotation directions. These structures are caused by the capillary force generated by evaporation of residual liquid between adjacent micropillars.

Measurement and Simulations of Vortical Dichroism. Optical vortices are generated by a spatial light modulator (SLM). The spatial light modulator has a resolution of 1920 × 1080 and a pixel spacing of 8 μm. The SLM operating in reflection mode can encode 256 grayscale programmable computer-generated holograms. After the vortex center is aligned with the chiral microstructure, a CCD camera is used to collect the surface reflection intensity. The reflection numerical simulation is carried out using finite difference software based on the time domain (Lumerical FDTD Solutions). In the simulation, the FDTD script function is used to establish the chiral structure model, which is consistent with the actual processing structure. For VD simulations, the incident light source was set as a linearly polarized vortex with a fixed wavelength of 800 nm and different topological charge numbers.

Characterization. SEM images are taken with a scanning electron microscope (EVO18, ZEISS), and optical images are taken with an inverted microscope. Optical microscopy (DMI 3000 B, Leica) and CCD (WV-BP334, Panasonic) are used to measure VD spectra.

ASSOCIATED CONTENT

Supporting Information

The Supporting Information is available free of charge at https://pubs.acs.org/doi/10.1021/acsnano.3c04181.

Deformation of hydrogel microstructures under different temperatures; capillary force analysis of smart hydrogel pillars; temperature-regulated reversible capillary force self-assembly; more details about experimental operations, results and discussions (PDF)

Video V1: dynamic deformation process of temperature response hydrogel cantilever beam (AVI)

Video V2: dynamic process of self-assembled chiral microstructures driven by capillary forces at different temperatures (AVI)

AUTHOR INFORMATION

Corresponding Authors

Zhaoxin Lao − *Anhui Province Key Laboratory of Measuring Theory and Precision Instrument, School of Instrument Science and Optoelectronics Engineering, Hefei University of Technology, Hefei 230009, China*; Email: laozx@hfut.edu.cn

Yanlei Hu − *CAS Key Laboratory of Mechanical Behavior and Design of Materials, Department of Precision Machinery and Precision Instrumentation, University of Science and Technology of China, Hefei 230027, China*; orcid.org/0000-0003-1964-0043; Email: huyl@ustc.edu.cn

Authors

Dong Wu − *CAS Key Laboratory of Mechanical Behavior and Design of Materials, Department of Precision Machinery and Precision Instrumentation, University of Science and Technology of China, Hefei 230027, China*; orcid.org/0000-0003-0623-1515

Caiding Ni − *CAS Key Laboratory of Mechanical Behavior and Design of Materials, Department of Precision Machinery and Precision Instrumentation, University of Science and Technology of China, Hefei 230027, China*

Yang Cao − *CAS Key Laboratory of Mechanical Behavior and Design of Materials, Department of Precision Machinery and Precision Instrumentation, University of Science and Technology of China, Hefei 230027, China*

https://doi.org/10.1021/acsnano.3c04181
ACS Nano XXXX, XXX, XXX−XXX

Jincheng Ni − *CAS Key Laboratory of Mechanical Behavior and Design of Materials, Department of Precision Machinery and Precision Instrumentation, University of Science and Technology of China, Hefei 230027, China*
Zhongguo Ren − *CAS Key Laboratory of Mechanical Behavior and Design of Materials, Department of Precision Machinery and Precision Instrumentation, University of Science and Technology of China, Hefei 230027, China*
Shunli Liu − *CAS Key Laboratory of Mechanical Behavior and Design of Materials, Department of Precision Machinery and Precision Instrumentation, University of Science and Technology of China, Hefei 230027, China*
Yuan Tao − *CAS Key Laboratory of Mechanical Behavior and Design of Materials, Department of Precision Machinery and Precision Instrumentation, University of Science and Technology of China, Hefei 230027, China*
Chen Xin − *Department of Mechanical and Automation Engineering, The Chinese University of Hong Kong, Hong Kong 999077, China*
Deng Pan − *Information Materials and Intelligent Sensing Laboratory of Anhui Province, Anhui University, Hefei 230601, China*
Jiaru Chu − *CAS Key Laboratory of Mechanical Behavior and Design of Materials, Department of Precision Machinery and Precision Instrumentation, University of Science and Technology of China, Hefei 230027, China;* orcid.org/0000-0001-6472-8103

Complete contact information is available at: https://pubs.acs.org/10.1021/acsnano.3c04181

Author Contributions

D. Wu, Z. Lao, and Y. Hu conceived the idea and developed the theory. C. Ni and J. Ni performed the simulations. C. Ni, Z. Lao, Y. Cao, Z. Ren, S. Liu, Y. Tao, C. Xin, and D. Pan performed the experiments. D. Wu, C. Ni, Z. Lao, and Y. Hu analyzed the data and wrote the manuscript. D. Wu, Z. Lao, Y. Hu, and J. Chu supervised the project. All authors discussed the results and commented on the manuscript.

Notes

The authors declare no competing financial interest.

ACKNOWLEDGMENTS

This work was supported by the National Natural Science Foundation of China (Grant Nos. 52175396, 52122511, 61927814, and 62205236), Major Scientific and Technological Projects in Anhui Province (202203a05020014), HFUT Basic Scientific Research Funds of Central Universities (JZ2022HGPA0312), and Youth Innovation Promotion Association CAS (Y2021118). The authors thank the USTC Center for Micro and Nanoscale Research and Fabrication.

REFERENCES

(1) Bishop, K. J.; Wilmer, C. E.; Soh, S.; Grzybowski, B. A. Nanoscale Forces and Their Uses in Self-Assembly. *Small* **2009**, *5*, 1600−1630.
(2) Kalsin, A. M.; Fialkowski, M.; Paszewski, M.; Smoukov, S. K.; Bishop, K. J.; Grzybowski, B. A. Electrostatic Self-Assembly of Binary Nanoparticle Crystals with a Diamond-Like Lattice. *Science* **2006**, *312*, 420−423.
(3) Randhawa, J. S.; Kanu, L. N.; Singh, G.; Gracias, D. H. Importance of Surface Patterns for Defect Mitigation in Three-Dimensional Self-Assembly. *Langmuir* **2010**, *26*, 12534−12539.
(4) Hatton, B.; Mishchenko, L.; Davis, S.; Sandhage, K. H.; Aizenberg, J. Assembly of Large-Area, Highly Ordered, Crack-Free Inverse Opal Films. *Proc. Natl. Acad. Sci. USA* **2010**, *107*, 10354−10359.
(5) Zhu, C.; Meng, G.; Zheng, P.; Huang, Q.; Li, Z.; Hu, X.; Wang, X.; Huang, Z.; Li, F.; Wu, N. A Hierarchically Ordered Array of Silver-Nanorod Bundles for Surface-Enhanced Raman Scattering Detection of Phenolic Pollutants. *Adv. Mater.* **2016**, *28*, 4871−4876.
(6) Stebe, K. J.; Lewandowski, E.; Ghosh, M. Oriented Assembly of Metamaterials. *Science* **2009**, *325*, 159−160.
(7) Lyu, D.; Xu, W.; Payong, J. E. L.; Zhang, T.; Wang, Y. Low-Dimensional Assemblies of Metal-Organic Framework Particles and Mutually Coordinated Anisotropy. *Nat. Commun.* **2022**, *13*, 3980−3990.
(8) Wang, H.; Chen, W.; Chen, B.; Jiao, Y.; Wang, Y.; Wang, X.; Du, X.; Hu, Y.; Lv, X.; Zeng, Y.; Wang, X.; Qian, L.; Xiong, J. Interfacial Capillary-Force-Driven Self-Assembly of Monolayer Colloidal Crystals for Supersensitive Plasmonic Sensors. *Small* **2020**, *16*, 1905480.
(9) Hu, Y.; Lao, Z.; Cumming, B. P.; Wu, D.; Li, J.; Liang, H.; Chu, J.; Huang, W.; Gu, M. Laser Printing Hierarchical Structures with the Aid of Controlled Capillary-Driven Self-Assembly. *Proc. Natl. Acad. Sci. USA* **2015**, *112*, 6876−6881.
(10) Lao, Z.; Pan, D.; Yuan, H.; Ni, J.; Ji, S.; Zhu, W.; Hu, Y.; Li, J.; Wu, D.; Chu, J. Mechanical-Tunable Capillary-Force-Driven Self-Assembled Hierarchical Structures on Soft Substrate. *ACS Nano* **2018**, *12*, 10142−10150.
(11) Lade, R. K., Jr; Jochem, K. S.; Macosko, C. W.; Francis, L. F. Capillary Coatings: Flow and Drying Dynamics in Open Microchannels. *Langmuir* **2018**, *34*, 7624−7639.
(12) Lee, K. K.; Ahn, C. H. A New On-Chip Whole Blood/Plasma Separator Driven by Asymmetric Capillary Forces. *Lab Chip* **2013**, *13*, 3261−3267.
(13) Paulsen, J. D.; Demery, V.; Santangelo, C. D.; Russell, T. P.; Davidovitch, B.; Menon, N. Optimal Wrapping of Liquid Droplets with Ultrathin Sheets. *Nat. Mater.* **2015**, *14*, 1206−1209.
(14) Karnaushenko, D.; Kang, T.; Bandari, V. K.; Zhu, F.; Schmidt, O. G. 3D Self-Assembled Microelectronic Devices: Concepts, Materials, Applications. *Adv. Mater.* **2020**, *32*, 1902994.
(15) Lam, C. H.; Chi, H.-Y.; Hsu, S.-M.; Li, Y.-S.; Lee, W.-Y.; Cheng, I. C.; Kang, D.-Y. Surfactant-Mediated Self-Assembly of Nanocrystals to Form Hierarchically Structured Zeolite Thin Films with Controlled Crystal Orientation. *RSC Adv.* **2017**, *7*, 49048−49055.
(16) Duan, T.; Ai, J.; Duan, Y.; Han, L.; Che, S. Self-Assembly of Chiral Nematic-Like Films with Chiral Nanorods Directed by Chiral Molecules. *Chem. Mater.* **2021**, *33*, 6227−6232.
(17) Miao, W.; Wang, D.; Liu, Z.; Tang, J.; Zhu, Z.; Wang, C.; Liu, H.; Wen, L.; Zheng, S.; Tian, Y.; Jiang, L. Bioinspired Self-Healing Liquid Films for Ultradurable Electronics. *ACS Nano* **2019**, *13*, 3225−3231.
(18) Jin, D.; Chen, Q.; Huang, T.-Y.; Huang, J.; Zhang, L.; Duan, H. Four-Dimensional Direct Laser Writing of Reconfigurable Compound Micromachines. *Mater. Today* **2020**, *32*, 19−25.
(19) Lao, Z.; Sun, R.; Jin, D.; Ren, Z.; Xin, C.; Zhang, Y.; Jiang, S.; Zhang, Y.; Zhang, L. Encryption/Decryption and Microtarget Capturing by PH-Driven Janus Microstructures Fabricated by the Same Femtosecond Laser Printing Parameters. *Int. J. Extreme Manuf.* **2021**, *3*, 025001.
(20) Hu, Y.; Yuan, H.; Liu, S.; Ni, J.; Lao, Z.; Xin, C.; Pan, D.; Zhang, Y.; Zhu, W.; Li, J.; Wu, D.; Chu, J. Chiral Assemblies of Laser-Printed Micropillars Directed by Asymmetrical Capillary Force. *Adv. Mater.* **2020**, *32*, 2002356.
(21) Liu, X.; Wei, M.; Wang, Q.; Tian, Y.; Han, J.; Gu, H.; Ding, H.; Chen, Q.; Zhou, K.; Gu, Z. Capillary-Force-Driven Self-Assembly of 4D-Printed Microstructures. *Adv. Mater.* **2021**, *33*, 2100332.
(22) Lao, Z.; Zheng, Y.; Dai, Y.; Hu, Y.; Ni, J.; Ji, S.; Cai, Z.; Smith, Z. J.; Li, J.; Zhang, L.; Wu, D.; Chu, J. Nanogap Plasmonic Structures Fabricated by Switchable Capillary-Force Driven Self-Assembly for

Localized Sensing of Anticancer Medicines with Microfluidic SERS. *Adv. Funct. Mater.* **2020**, *30*, 1909467.
(23) Ansell, H. S.; Kim, D. S.; Kamien, R. D.; Katifori, E.; Lopez-Leon, T. Threading the Spindle: A Geometric Study of Chiral Liquid Crystal Polymer Microparticles. *Phys. Rev. Lett.* **2019**, *123*, 157801.
(24) Winogradoff, D.; Li, P. Y.; Joshi, H.; Quednau, L.; Maffeo, C.; Aksimentiev, A. Chiral Systems Made from DNA. *Adv. Sci.* **2021**, *8*, 2003113.
(25) Buchanan, K. A.; Lakes, R. S.; Vanderby, R. Jr. Chiral Behavior in Rat Tail Tendon Fascicles. *J. Biomech.* **2017**, *64*, 206−211.
(26) Su, X.; Zhu, D.; Zheng, C.; Tomovic, M. M. Mechanical Properties of 65Mn Chiral Structure with Three Ligaments. *Acta Mech. Sin.* **2019**, *35*, 88−98.
(27) Wang, M.; Lin, B. P.; Yang, H. A Plant Tendril Mimic Soft Actuator with Phototunable Bending and Chiral Twisting Motion Modes. *Nat. Commun.* **2016**, *7*, 13981−13988.
(28) Zhao, Y.; Askarpour, A. N.; Sun, L.; Shi, J.; Li, X.; Alu, A. Chirality Detection of Enantiomers Using Twisted Optical Metamaterials. *Nat. Commun.* **2017**, *8*, 14180−14187.
(29) Pokroy, B.; Kang, S. H.; Mahadevan, L.; Aizenberg, J. Self-Organization of a Mesoscale Bristle into Ordered, Hierarchical Helical Assemblies. *Science* **2009**, *323*, 237−239.
(30) Apsite, I.; Salehi, S.; Ionov, L. Materials for Smart Soft Actuator Systems. *Chem. Rev.* **2022**, *122*, 1349−1415.
(31) Zhang, Y. L.; Tian, Y.; Wang, H.; Ma, Z. C.; Han, D. D.; Niu, L. G.; Chen, Q. D.; Sun, H. B. Dual-3D Femtosecond Laser Nanofabrication Enables Dynamic Actuation. *ACS Nano* **2019**, *13*, 4041−4048.
(32) Kim, J.; Im, S.; Kim, J. H.; Kim, S. M.; Lee, S. M.; Lee, J.; Im, J. P.; Woo, J.; Moon, S. E. Artificial Perspiration Membrane by Programmed Deformation of Thermoresponsive Hydrogels. *Adv. Mater.* **2020**, *32*, 1905901.
(33) Sutton, A.; Shirman, T.; Timonen, J. V.; England, G. T.; Kim, P.; Kolle, M.; Ferrante, T.; Zarzar, L. D.; Strong, E.; Aizenberg, J. Photothermally Triggered Actuation of Hybrid Materials As a New Platform for in Vitro Cell Manipulation. *Nat. Commun.* **2017**, *8*, 14700−14711.
(34) Zhao, Y.; Lo, C.-Y.; Ruan, L.; Pi, C.-H.; Kim, C.; Alsaid, Y.; Frenkel, I.; Rico, R.; Tsao, T.-C.; He, X. Somatosensory Actuator Based on Stretchable Conductive Photothermally Responsive Hydrogel. *Sci. Rob.* **2021**, *6*, No. eabd5483.
(35) Dong, M.; Shi, B.; Liu, D.; Liu, J. H.; Zhao, D.; Yu, Z. H.; Shen, X.; Gan, J. M.; Shi, B. L.; Qiu, Y.; Wang, C. C.; Zhu, Z. Z.; Shen, Q. D. Conductive Hydrogel for a Photothermal-Responsive Stretchable Artificial Nerve and Coalescing with a Damaged Peripheral Nerve. *ACS Nano* **2020**, *14*, 16565−16575.
(36) Hippler, M.; Blasco, E.; Qu, J.; Tanaka, M.; Barner-Kowollik, C.; Wegener, M.; Bastmeyer, M. Controlling the Shape of 3D Microstructures by Temperature and Light. *Nat. Commun.* **2019**, *10*, 232−239.
(37) Qian, X.; Zhao, Y.; Alsaid, Y.; Wang, X.; Hua, M.; Galy, T.; Gopalakrishna, H.; Yang, Y.; Cui, J.; Liu, N.; Marszewski, M.; Pilon, L.; Jiang, H.; He, X. Artificial Phototropism for Omnidirectional Tracking and Harvesting of Light. *Nat. Nanotechnol.* **2019**, *14*, 1048−1055.
(38) Pasparakis, G.; Tsitsilianis, C. LCST Polymers: Thermoresponsive Nanostructured Assemblies Towards Bioapplications. *Polymer* **2020**, *211*, 123146.
(39) Duan, H.; Yang, J. K.; Berggren, K. K. Controlled Collapse of High-Aspect-Ratio Nanostructures. *Small* **2011**, *7*, 2661−2668.
(40) Duan, H.; Berggren, K. K. Directed Self-Assembly at the 10 nm Scale by Using Capillary Force-Induced Nanocohesion. *Nano Lett.* **2010**, *10*, 3710−3716.
(41) Kim, I.; Mun, J.; Hwang, W.; Yang, Y.; Rho, J. Capillary-Force-Induced Collapse Lithography for Controlled Plasmonic Nanogap Structures. *Microsyst. Nanoeng.* **2020**, *6*, 65−73.
(42) Ni, J.; Liu, S.; Wu, D.; Lao, Z.; Wang, Z.; Huang, K.; Ji, S.; Li, J.; Huang, Z.; Xiong, Q.; Hu, Y.; Chu, J.; Qiu, C. W. Gigantic Vortical Differential Scattering As a Monochromatic Probe for Multiscale Chiral Structures. *Proc. Natl. Acad. Sci. USA* **2021**, *118*, No. e2020055118.
(43) Ni, J.; Wang, C.; Zhang, C.; Hu, Y.; Yang, L.; Lao, Z.; Xu, B.; Li, J.; Wu, D.; Chu, J. Three-Dimensional Chiral Microstructures Fabricated by Structured Optical Vortices in Isotropic Material. *Light: Sci. Appl.* **2017**, *6*, No. e17011.
(44) Hu, Y.; Feng, W.; Xue, C.; Lao, Z.; Ji, S.; Cai, Z.; Zhu, W.; Li, J.; Wu, D.; Chu, J. Self-Assembled Micropillars Fabricated by Holographic Femtosecond Multi-Foci Beams for in Situ Trapping of Microparticles. *Opt. Lett.* **2020**, *45*, 4698−4701.

https://doi.org/10.1021/acsnano.3c04181
ACS Nano XXXX, XXX, XXX−XXX